Abstract

In recent decades, the central North Sea has been experiencing a general trend of decreasing dissolved oxygen (O_2) levels during summer. To understand potential causes driving lower O_2, we investigated a three-day period of summertime turbulence and O_2 dynamics in the thermocline and bottom boundary layer (BBL). The study focuses on coupling biogeochemical with physical transport processes to identify key drivers of the O_2 and organic carbon turnover within the BBL. Combining our flux observations with an analytical process-oriented approach, we resolve drivers that ultimately contribute to determining the BBL O_2 levels. We report substantial turbulent O_2 fluxes from the thermocline into the otherwise isolated bottom water attributed to the presence of a baroclinic near-inertial wave. This transient contribution to the local bottom water O_2 and carbon budgets has been largely overlooked and is shown to play a role in promoting high carbon turnover in the bottom water while simultaneously maintaining high O_2 concentrations. This process could become suppressed with warming climate and stronger stratification, conditions which may promote migrating algal species that could potentially shift the O_2 production zone higher up within the thermocline.

1 Introduction

1.1 Hypoxia in shelf seas and coastal regions

The distribution of dissolved oxygen (O_2) in marine systems results from a complex interaction between biological processes (photosynthesis and respiration) and physical processes (O_2 flux pathways) occurring within the water column and at the seafloor. O_2 is regarded as an important indicator of ecosystem functioning for aquatic organisms (Best et al., 2007) and for benthic activity (e.g., Glud, 2008). Changes in O_2 distribution, concentrations and supply can therefore have severe impacts on shelf ecosystems. O_2 concentrations below 62.5 μmol L^{-1}, which is generally regarded as the threshold of hypoxia (Vaquer-Sunyer and Duarte, 2008), are shown to significantly stress aquatic communities and increase the mortality among fish communities (Diaz, 2001). These ecological and economic impacts of O_2 depletion lead to increasing concern regarding hypoxia occurrence and hypoxic events. As reviewed by Diaz and Rosenberg (2008), hypoxia in coastal environments is spreading and so are the reports of unprecedented occurrence of hypoxia in several

shelf seas and coastal regions (Grantham et al., 2004; Chan et al., 2008; Crawford and Pena, 2013).

1.2 Hydrodynamics and oxygen depletion in the North Sea

The North Sea is situated on the North–West European continental shelf, between the British Islands and continental Europe (Fig. 1). Its semi-enclosed basin covers an area of 575'300 km^2, with an average depth of 74 m and a general decrease in depth from North to South (Otto et al., 1990). The central region is characterized by the presence of the Dogger Bank, a shallow sandbank that acts as a hydrological divide. The northern and central North Sea hydrology is mainly dominated by inflow from the North Atlantic Ocean at the northern open boundary, while the southern part relies on inflow from the English Channel (Thomas et al., 2005). Northern and central North Sea areas are characterized by seasonal water column stratification (April to September - October; Meyer et al., 2011). With only weak, wind-driven residual currents (Otto et al., 1990), this stratification leads to isolation of central North Sea bottom water and subsequent O_2 depletion.

In the central North Sea, the occurrence of low O_2 levels in bottom waters has been reported (e.g., North Sea Task Force, 1993; Greenwood et al., 2010). Additional monitoring studies in the central North Sea in 2007 and 2008 have shown that O_2 concentration in bottom waters at the Oyster Grounds and North Dogger can drop to 163 – 169 μmol L^{-1} (60 – 63% saturation) and ~200 μmol L^{-1} (71% saturation), respectively (Fig. 1; Greenwood et al., 2010). Comparable field observations were also reported in the summer of 2010 (Queste et al., 2013). The authors also reviewed the available historical O_2 data in the North Sea (1900 – 2010), revealing a clear increase in O_2 depletion after 1990.

While the reported O_2 levels were still above the hypoxic threshold, growing concerns of hypoxia developing in the North Sea have highlighted the need for more detailed studies on O_2 dynamics and its driving forces (Kemp et al., 2009). Since 1984, surface water temperatures in the North Sea have increased by 1 – 2°C, greater than the global mean (OSPAR, 2009, 2010; Meyer et al., 2011). On seasonal time scales, climate projections indicate longer durations of the stratification period and stronger thermocline stability (Lowe et al., 2009; Meire et al., 2013), with some projections suggesting earlier onset of stratification (e.g., Lowe et al., 2009). Due to

the semi-enclosed nature of the North Sea, earlier onset and longer stratification increases the length of time that deep waters are isolated, potentially allowing lower O_2 concentrations to develop (Greenwood et al., 2010).

1.3. Physical drivers of oxygen dynamics

The distribution of O_2 and other dissolved constituents within aquatic systems are largely driven by physical transport processes. These include wind driven air – water gas exchange at the sea surface (Wanninkhof, 1992), molecular diffusion at the sediment – water interface (Jørgensen and Revsbech, 1985), horizontal advection (e.g., Radach and Lenhart, 1995) and turbulent transport in the water column, where the latter transport was reported to significantly contribute to constituent balances (see Rippeth, 2005; Fischer et al., 2013; Kreling et al., 2014; Brandt et al., 2015). In shelf seas, the seasonal occurrence of steep thermoclines acts as an important physical barrier separating the surface layer from nutrient-rich deeper waters (Sharples et al., 2001). As measurements of shear and stratification have shown, the central North Sea thermocline is in a state of marginal stability (van Haren et al., 1999). Hence additional sources of shear could trigger shear instability leading to local production of turbulence within the thermocline. This enhanced local turbulence would subsequently enhance the vertical exchange of constituents such as O_2, organic carbon and nutrients. Resolving processes that drive diapycnal (i.e., vertical) fluxes across the thermocline throughout the stratification period is key to understanding the biogeochemical functioning of shelf seas (e.g., Sharples et al., 2001).

1.4 Present study

The goal of this study is to provide understanding of key turbulent processes driving O_2 fluxes across the thermocline during the summertime stratification period in the central North Sea using data from a 3-day process study. We investigate and describe O_2 dynamics and fluxes to the bottom waters and discuss their potentially influence on the seasonal O_2 balance. Using the resolved O_2 fluxes, we perform a simple 1-D mass balance model to quantify O_2 sources and sinks. Finally, processes that could further promote hypoxia in the central North Sea in a warming climate are discussed.

2 Methods

2.1 Study site

We performed O_2 and turbulence measurements in the Norwegian sector of the central North Sea, N. 1/9, at the Tommeliten site (56°29'30" N, 2°59'00" E; Fig. 1) from 8 – 11 August 2009 aboard the R/V *Celtic Explorer* (cruise CE0913). The site, located ~100 km northeast from the northern Dogger Bank, and its surroundings are characterized by shallow waters (~70 m) relatively far from coastal areas (on average ~300 km). The site is known for the presence of buried salt diapirs, methane (CH_4) seeps and bacterial mats (Hovland and Judd, 1988). Bathymetric surveys from Schneider von Deimling et al. (2010) revealed a rather flat sandy seabed with almost no features, with the exception of cm-sized ripples (McGinnis et al., 2014).

The currents of the central North Sea are predominantly driven by the semi-diurnal lunar tide (M_2) (Otto et al., 1990). Seasonal stratification begins in April around Julian day 100 and lasts until the end of September or early October, Julian days 270- 290 (e.g. Meyer et al., 2011). The thermocline has been identified as an important zone for the establishment of primary production and the O_2 maximum layer (see Pingree et al., 1978). In fact, the North Sea deep chlorophyll maximum (DCM) is estimated to account for 58% of the water column primary production and 37% of the annual new production for the summer stratified North Sea (Weston et al., 2005). The development of the associated O_2 maximum due to this production is thus important and so far not considered in the overall O_2 balance of the central North Sea.

2.2 Instrumental setup

High resolution (mm scale) turbulent shear and temperature profiles were obtained with a MSS90-L microstructure turbulence profiler (Sea and Sun Technology, Trappenkamp, Germany). The MSS90-L is a free-falling, loosely-tethered profiler which samples at 1024 Hz with 16 channels and is designed for an optimal sink rate of 0.5 – 0.6 m s^{-1}. The probe was equipped with two air-foil shear probes, an accelerometer (to correct for probe pitch, roll, and vibration), a fast temperature sensor (FP07, 7–12 ms response time), standard CTD sensors (temperature, pressure, conductivity), and a fast (0.2 s response time) galvanic O_2 sensor (AMT, Analysenmesstechnik GmbH, Rostock, Germany). Absolute O_2

concentrations were calibrated against shipboard CTD O_2 profiles and Winkler titrations using discrete water samples (see below).

Water column hydrodynamics were characterized with the compact benthic Paleoceanography (POZ) lander, which was deployed using a video guided launcher (Pfannkuche and Linke, 2003). The POZ lander recorded 3-dimensional current velocity profiles and acoustic backscatter information throughout the water column using a 300 kHz acoustic Doppler current profiler (ADCP; Workhorse Sentinel, Teledyne RD Instruments, Poway, United States), which sampled every 15 s with a bin size of 0.5 m starting from 2.75 m from the bottom. A conductivity-temperature-depth (CTD) logger (XR-420 CT logger, RBR, Kanata, Canada) recorded temperature, conductivity and pressure (Digiquarz, Paroscientific, Redmond, United States) every 2 s near the seafloor (~0.3 m distance). The POZ lander was also equipped with a Winkler–calibrated O_2 optode sensor (Aanderaa Data Instruments AS, Bergen, Norway), which recorded BBL O_2 concentration at 1 min intervals.

Water column profiles were obtained using a SBE9plus CTD-rosette system (Seabird, Washington, United States). The CTD sampled at 24 Hz and was equipped with standard temperature, conductivity, pressure, O_2 and light transmission sensors. The rosette system mounted 12 Niskin bottles (10 L each) for discrete water sampling. Each water sample was subsampled with three Winkler bottles of known volume (~62 mL on average) upon recovery, and the samples were immediately fixed on deck and titrated manually within 24 h after the sampling (see Winkler 1888). CTD O_2 concentrations deviated from Winkler values by <5%.

2.3 Hydrodynamic data evaluation

The main tidal directions (major and minor axis of the tidal ellipsoid) were determined by performing a variance analysis on the ADCP velocity time series. The u and v velocities were rotated over a stepwise increasing rotation angle (r) as $u_{rot} = u \cdot cos(-r) - v \cdot sin(-r)$ and $v_{rot} = u \cdot sin(-r) - v \cdot cos(-r)$, and the variance computed at each step. The angle with the largest variance is the main tidal direction. Barotropic and baroclinic flow contributions of tides were separated by least-square fitting the detrended velocity time series to harmonics $u = A \cdot cos(\omega \cdot t + \varphi)$ with A, ω, φ being the amplitude, frequency, and the phase lag, respectively. In the analysis below, the barotropic semi-diurnal principle lunar tide (M_2) and

diurnal declination tide (K_1) contributions had frequencies of 1.93227 cycles per day (cpd) and 1.00274 cpd, respectively, and were subtracted from the time series to analyze residual flow. For barotropic contributions, the fit was applied to the depth average of the time series, while baroclinic contributions were obtained by fitting the harmonics to the velocity time series from each 0.5 m ADCP bin. The occurrence of enhanced shear in the stratified water column was investigated by calculating the vertical shear of horizontal velocity, *S*, from the vertical gradients between adjacent bins of east and north velocity (0.5 m resolution) as $S = \sqrt{(du/dz)^2 + (dv/dz)^2}$. Frequency spectra of the time series of horizontal velocity and vertical shear of horizontal velocity were used to identify the tidal and non-tidal flow components. The spectra were calculated using fast-Fourier transforms combined with a ½-cosine tapper (Hanning window), which was applied to the first and last 10% of the time series data.

Turbulent kinetic energy dissipation rate (ε) was quantified from airfoil shear readings by integrating shear wavenumber spectra assuming isotropic turbulence (Batchelor, 1953):

$$\varepsilon = 7.5\mu \int_{k_{min}}^{k_{max}} E_{du'/dz}(k)dk \quad (1)$$

where μ is the dynamic viscosity of seawater. Shear spectra $E_{du'/dz}(k)$ were calculated from one-second ensembles (1024 values) and integrated between a lower $k_{\min}$ = 3 cycles per minute (cpm) and an upper wavenumber $k_{\min}$ that varied between 14 cpm and 30 cpm depending on the Kolmogorov wavenumber. Here, a Bartlett window was applied to the whole ensemble prior to spectral decomposition. Loss of variance due to limited wavenumber band was taken into account by fitting the observed shear spectra to the universal Nasmyth spectrum. Similarly, corrections for the loss of variance due to finite sensor tip of the airfoil probes were applied (see Schafstall et al., 2010). The detection limit, or noise level, of the used profiler for ε was inferred to be 1×10^{-9} W kg^{-1} (Schafstall et al., 2010); the upper detection limit is a function of the shear sensor geometry (up to 10^{-4} W kg^{-1}; Prandke and Stips, 1998).

Estimates of turbulent eddy diffusivities of mass (K_ρ) were obtained from measurements of ε as

$$K_\rho = \gamma\varepsilon/N^2 \quad (2)$$

where γ is the mixing efficiency and N^2 the water column stability. This method, proposed by Osborn (1980), approximates K_ρ under the assumption of a local equilibrium of production and dissipation of turbulent kinetic energy. Values for N^2 were calculated from temperature, salinity and pressure data using the adiabatic method (Fofonoff, 1985) as $N^2 = -\mathrm{g}(\rho^{-1}\partial\rho/\partial z - g/c^2)$, where ρ, g, and c are the density, the earth's gravitational acceleration and speed of sound. Mixing efficiency values in stratified waters range from 0.1 to 0.2 (Ivey and Imberger, 1991) and decreases in weakly stratified waters such as within the BBL (Lorke et al., 2008). To account for this decrease, we used the γ and K_ρ parameterization of Shih et al. (2005). Based on the turbulence activity parameter $\varepsilon/\upsilon N^2$, with the kinematic viscosity, υ, the authors found that in energetic regimes, i.e., $\varepsilon/\upsilon N^2 > 100$, eddy diffusivities are better estimated as $K_\rho = 2\upsilon(\epsilon/\upsilon N^2)^{1/2}$. As horizontal density gradients at the study site were deemed to be small compared to vertical gradients (see Discussion), we equated diapycnal eddy diffusivities with vertical diffusivities (i.e., $K_\rho = K_z$).

To obtain representative mean turbulent eddy diffusivities, the data were evaluated in ensembles of three to four consecutive profiles and averaged in depth and time to reduce uncertainties due to the patchiness of turbulence, temporal fluctuation of N^2, and temporal γ variations (see Smyth et al., 2001). As proposed by Ferrari and Polzin (2005), the level of uncertainty of the averaged K_z can be quantified as:

$$\Delta K_z = K_z \left[\left(\frac{\Delta\gamma}{\gamma}\right)^2 + \left(\frac{\Delta\varepsilon}{\varepsilon}\right)^2 + \left(\frac{\Delta N^2}{N^2}\right)^2 \right]^{1/2} \quad (3)$$

with Δ being the absolute uncertainty of the various average terms. Here, the uncertainties are evaluated in the region of strong vertical O_2 gradients and in 2 m depth bins. The absolute uncertainty for $\Delta\gamma$ was assumed to be 0.04 (see St. Laurent and Schmitt, 1999). The absolute uncertainty on N^2 (ΔN^2) was determined by the standard error over the 2 m average, computed as the standard deviation divided by the square root of the number of estimates. Finally, the statistical uncertainty of ε for each bin was calculated using a bootstrap method (10^4 resamples) (Efron, 1979).

The vertical O_2 fluxes F_θ were then obtained from K_z and the O_2 concentration gradients $\partial[O_2]/\partial z$ as

$$F_\theta = K_z \frac{\partial[O_2]}{\partial z} \quad (4)$$

Accordingly, the uncertainty of averaged turbulent O_2 fluxes were given by:

$$\Delta F_\theta = F_\theta \left[\left(\frac{\Delta K_z}{K_z} \right)^2 + \left(\frac{\Delta \partial_z [O_2]}{\partial_z [O_2]} \right)^2 \right]^{1/2} \quad (5)$$

where $\Delta \partial_z [O_2]$ denotes the standard error of mean vertical gradients of O_2 concentrations. It should be noted that the analysis did not include biases or uncertainties due to measurement errors.

3 Results

During the three-day observational period (8 – 11 August 2009), we collected 39 high-resolution MSS profiles in consecutive sets of three to five profiles at 5 – 10 min intervals. Most of the profiles were in the evening (profiles 1 – 8, 26 – 28, 36 – 39) or at night (9 – 15, 29 – 35) with the remaining profiles acquired in the morning (6 to 9 AM). One shipboard CTD profile was performed prior to the actual MSS profiles to provide hydrographic information, the water turbidity and O_2 concentrations, and discrete water samples for subsequent onboard Winkler titrations. Hydroacoustic water column current measurements were carried out continuously throughout the observational period. The following results are structured to first present a characterization of the site's physical settings and turbulence drivers, followed by the O_2 fluxes and O_2 BBL budget.

3.1 Water column structure

The ~70 m deep water column was characterized by a stable, well-defined four-layer temperature structure (Fig. 2a). The well-mixed surface boundary layer (SBL) and bottom boundary layer (BBL), 15 m and 30 m thick, respectively, were separated by a weakly-stratified transition layer (15 – 25 m depth) and a strongly stratified interior layer (25 – 40 m depth). The stratified interior layer was characterized by two very steep thermoclines situated in the upper (27 – 30 m depth) and lower (36 – 39 m depth) region of the layer, with vertical temperature gradients of up to 4°C m^{-1}. The average salinity was 35.08 with little variation throughout the water column (35.04 – 35.1). The light transmission profile from the ship CTD ranged from 89% to 96% (Fig. 2b). The most turbid layer (89%) was observed at the lower boundary of the interior layer (at 40 m depth) suggesting the presence of the deep chlorophyll maximum, phytoplankton, zooplankton and suspended particles.

253 The O_2 profiles were generally characterized by near saturation in the SBL
254 and transition layers (238 – 243 µmol kg^{-1}) and undersaturated (~80%) in the BBL
255 (~243 µmol kg^{-1}) (Fig. 2c,d). The stratified interior was oversaturated by up to 115%,
256 with a well-established O_2 maximum at ~39 m depth with concentrations up to ~315
257 µmol kg^{-1}. Below that maximum, at the thermocline-BBL interface, we observed a 2 –
258 3 m thick steep oxycline, with an O_2 gradient of 34 µmol kg^{-1} m^{-1} and exhibiting very
259 limited day/night, depth and thickness variation. We resolve the O_2 flux into the BBL
260 associated with this oxycline.
261
262 **3.2 Hydrodynamics**

263 The hydrostatic pressure dataset (POZ lander) revealed that the tidal water
264 level ranged from 0.6 to 0.9 m (Fig. 3a). Variance analysis on the ADCP velocity data
265 identified the major and minor axis of the tidal ellipsoid components to occur at 45°
266 and 135° from true north, respectively. Along these axes, the current amplitudes were
267 0.21 m s^{-1} and 0.04 m s^{-1}, indicating a narrow tidal current ellipsoid, as reported by
268 Otto et al. (1990). The site was characterized by a negative tide polarity (anti-
269 cyclonic) for the semi-diurnal tides. A dominance of the barotropic M_2 current
270 amplitude at all depths was clearly visible in the velocity time series (Fig. 3b, c) and
271 the harmonic analyses. East (zonal) and north (meridional) barotropic M_2-current
272 amplitudes were 0.12 m s^{-1} and 0.17 m s^{-1}, respectively, while K_1-current amplitudes
273 were only 0.005 m s^{-1} and 0.03 m s^{-1}.

274 Although the limited length of the ADCP velocity time series did not allow for
275 full separation of the M_2 and *f* frequencies, the spectral density functions indicated
276 maximum energy at frequencies of about the semi-diurnal tide. This maximum varied
277 little with depth, indicating barotropic M_2 motions. Superimposed on those barotropic
278 currents, we observed the presence of baroclinic velocity contributions (Fig. 3b, c).
279 Additionally, near-inertial motions were also detected.

280 The occurrence of near-inertial motions was most pronounced in the
281 thermocline (32 – 39 m; Fig. 3e). Lower, but still elevated, energy densities at the
282 near-inertial band were found in the SBL and BBL. Moreover, the near-inertial
283 currents exhibited a distinct 180° phase shift between the SBL and the thermocline as
284 well as between the thermocline and the BBL, suggesting a second vertical mode
285 nature of these fluctuations. Average amplitudes of the near-inertial fluctuations in the

thermocline obtained from least-square fitting were 0.11 m s^{-1}. In the BBL and SBL, average amplitudes were reduced to 0.06 m s^{-1} and 0.04 m s^{-1}, respectively, suggesting that *f* oscillations might account for enhanced shear in the thermocline.

Enhanced vertical shear of horizontal velocity was found at the interior – transition layer and at the interior – BBL interfacial regions (Fig. 3d). As indicated by the spectral density function of the shear time series from the interior interfacial layers (SI Fig. 1), the shear exhibited near-inertial frequencies (1.6722 cpd), and resulted from the baroclinic near-inertial wave. The high vertical resolution (0.5 m) of our velocity data allowed the resolution of the interfacial shear layers, which were typically 2 to 3 m thick with elevated values of up to 0.05 s^{-1}. Comparisons with CTD data showed that they are collocated with the two enhanced temperature gradients layers in the thermocline (27 – 30 m and 36 – 39 m depth; Fig. 2a).

The dissipation rates (ε) of turbulent kinetic energy (TKE) determined from microstructure shear probes were particularly low in the center of the stratified interior ($2 - 5 \times 10^{-9}$ W kg^{-1}) but still above the MSS detection limit. However, ε increased to 5×10^{-9} W kg^{-1} and 2×10^{-8} W kg^{-1} at the upper and lower interior layer limits, respectively (Fig. 4a). These coincided with the depth range of the interfacial shear layers (Fig. 3d) at the strong temperature gradients (Fig. 2a) and resulting water column stability maxima ($\sim 1 \times 10^{-3}$ s^{-2}).

Bin-averaged values of K_z varied by a factor of 5, ranging from 6×10^{-7} m^2 s^{-1} in the central interior to 3×10^{-6} m^2 s^{-1} in the lower region of the transition layer (Fig. 4b). In the upper interface (thermocline – transition layer), where ε was elevated with respect to the central interior but reduced compared to the lower interfacial layer, stronger stratification (i.e., larger N^2 values up to 10^{-3} s^{-2}) reduced the eddy diffusivities. At the interior-BBL, higher K_z values ($\sim 2 \times 10^{-5}$ m^2 s^{-1}) resulted from increased turbulence and weaker stratification. This enhanced turbulent transport was located where the vertical O_2 gradient was the strongest (Fig. 2d).

3.3 Oxygen fluxes and budget

With the fast responding AMT galvanic O_2 sensor and rapid sampling rate, we were able to resolve the O_2 gradient with high precision. Figure 4c shows the 2 m bin average O_2 fluxes for the interior together with the averages from each ensemble.

Small O_2 fluxes (~1 mmol m^{-2} d^{-1}) were estimated for the center and upper region of the interior; suggesting that relatively little O_2 is transported upward from the O_2 maximum to the upper interior. In contrast, a substantial O_2 flux ranging from 9 – 134 mmol m^{-2} d^{-1} (average of 54 mmol m^{-2} d^{-1}) was identified from the lower thermocline towards the BBL. The confidence interval associated with the uncertainties of the O_2 flux estimates was 18 – 74 mmol m^{-2} d^{-1}. Although the O_2 fluxes to the BBL water from the thermocline were variable in magnitude (Fig. 4c) and the measurements limited to the observational period (Fig. 3), their magnitude nevertheless suggests an important, yet overlooked, O_2 pathway.

We performed a simple 1-D BBL mass balance to investigate the relevance to the local O_2 balance during our observational period. Here, we defined the apparent (measured) O_2 loss rate in the BBL $\partial[O_2]/\partial t$ as the consequence of O_2 replenishment from F_θ and the O_2 utilization via sediment O_2 uptake rate (*SUR*) and water column organic matter respiration (*R*) expressed as

$$\frac{\partial[O_2]}{\partial t}\frac{V}{A} = |F_\theta| - |SUR| - |R| \quad \{mmol\ m^{-2}\ d^{-1}\} \tag{6}$$

The mass balance was constrained to the (assumed) well-mixed 35 m deep BBL section of area, A = 1 m^2 with a volume V = 35 m^3. We further assumed negligible horizontal O_2 gradients (as observed from the CTD casts), and thus a net zero horizontal O_2 advective transport.

The average *SUR* for the same time period and location, obtained from parallel eddy correlation measurements, was ~-10 mmol m^{-2} d^{-1} (McGinnis et al., 2014). The *SUR* was consistent with the average *SUR* at Oyster Grounds reported by Neubacher et al. (2011), -9.8 mmol m^{-2} d^{-1}, and with modeled *SUR*s at the same site (average -8.6 mmol m^{-2} d^{-1}; Meire et al., 2013). The apparent BBL O_2 loss of -0.42 µmol kg^{-1} d^{-1} was determined from the POZ lander O_2 optode time series (Fig. 5a) over 52 hours, (R^2=0.60). Though limited to our short observational period, the vertically integrated apparent BBL O_2 loss was about -15 mmol m^{-2} d^{-1} and thus within 2% of the nearby North Dogger average presented by Greenwood et al. (2010). Based on Eq. (6) and using the observed BBL O_2 loss rate, F_θ and *SUR*, the water column respiration, *R* was calculated to be ~-60 mmol m^{-2} d^{-1}. This implies that without the O_2 replenishment, the apparent BBL O_2 loss would be ~-2 µmol kg^{-1} d^{-1} and thus four times higher than observed. Our results indicated that the total respiration in the

bottom water was therefore ~-70 mmol m^{-2} d^{-1} (*SUR* + *R*), with about 14% of the organic carbon mineralization occurring in the sediment and 86% in the BBL.

4 Discussion

During our three-day observational period, we found that the baroclinic near-inertial wave in the interior was the main contributor to the detected enhanced shear (Fig. 3d) and the observed elevated vertical O_2 flux to the BBL (Fig. 6). As near-inertial waves decay after a few weeks, it should be noted that we observed a rather special situation, and that vertical O_2 fluxes will not likely be as highly elevated during periods when near-inertial waves are not present.

Within this context, we: 1) discuss the turbulent mechanisms leading to these thermocline O_2 fluxes and mechanisms promoting the formation of the O_2 maximum zone in terms of primary productivity; 2) discuss the implication for the local O_2 BBL dynamics and carbon budget; 3) elaborate on factors that can ultimately influence O_2 depletion in the North Sea and other seasonally stratified shelf seas.

4.1 Thermocline mixing

The expansive North Sea thermocline ($1 - 5 \times 10^5$ km^2; Meyer et al., 2011) has been regarded as being in a state of marginal stability, where additional sources of shear could lead to increased thermocline mixing (e.g., van Haren et al., 1999). Itsweire et al. (1989) showed that layers of strong shear are likely to be found where strong stratification occurs. Generally, in the absence of varying topography and sloping boundaries, the major sources of shear in the thermocline are considered to be internal tides and near-inertial oscillations (see Rippeth, 2005). Sharples et al. (2007) demonstrated that internal tidally-driven thermocline mixing enhanced diapycnal nutrient fluxes, the overall productivity in the thermocline, and the associated carbon export to the BBL.

The occurrence of near-inertial oscillations in shelf seas during the stratified season has been reported in several studies from the North Sea (van Haren et al., 1999; Knight et al., 2002) and in other shelf seas (e.g., Rippeth et al., 2002; McKinnon and Gregg, 2005). During the presence of baroclinic inertial waves in the water column, periods of enhanced shear have been observed in the western Irish Sea

(Rippeth et al., 2009), the Celtic Sea (Palmer et al., 2008) and the northern North Sea (Burchard and Rippeth, 2009). These take the form of shear spikes, which occur approximately every inertial period and in bursts lasting several days.

While we mainly attributed the observed enhanced turbulent mixing to the occurrence of a near-inertial wave, the site's physical setting has further implications for mixing processes in the thermocline. In the northern hemisphere, sites with anti-cyclonic tides, such as Tommeliten, are often characterized by an increased vertical extension of the BBL, and higher BBL dissipation rates than comparable cyclonic sites (see Simpson and Tinker, 2009). As a result of this enhanced BBL thickness, we observed sporadically elevated thermocline turbulence resulting from tidal-driven bottom turbulence propagating vertically towards the thermocline (Fig. 5b). A study by Burchard and Rippeth (2009) also reported that short lived thermocline shear spikes can arise due to the alignment of the surface wind stress, bulk shear, and bed stress vectors in the presence of baroclinic near-inertial motions and barotropic tidal currents. These mechanisms are stronger with anti-cyclonic tides. Although all the features required for shear spike generation were present during the observational period, the two-layer mechanism described by these authors would require a more complex water column structure to be applicable to the Tommeliten site.

The site's water column structure clearly showed the occurrence of a 10 m thick transition layer (Fig. 2a). This layer represents the region of the water column where mixing turns from elevated in the SBL to strongly reduced in the interior (Ferrari and Boccaletti, 2004). The transition layer is therefore an obligate pathway for solute and heat exchange between SBL and the interior (Ferrari and Boccaletti, 2004; Rhein et al., 2010) and has been reported to be a region of enhanced shear and near-inertial wave activity (Dohan and Davis, 2011). Although the presented data did not allow quantification of the O_2 exchange across the transition layer, such contribution might be considerable and thus highly relevant for the cycling of O_2 and CO_2 in the upper water column, which in turn could have direct biological implications.

4.2 BBL O_2 dynamics

Ultimately, observed O_2 depletion in the BBL of the central North Sea depends on the supply of organic matter, the rate of carbon mineralization, and the

flux of O_2 to the bottom water either from horizontal advection or turbulent vertical transport. Our study investigated the significance of turbulent vertical O_2 fluxes to the BBL, which has been previously overlooked in shelf sea carbon balances. Studies focusing on O_2 replenishment in the BBL through the thermocline are limited to freshwater systems (e.g. Bouffard et al., 2013; Kreling et al., 2014). In a large stratified water body such as Lake Erie, O_2 transport from the thermocline to the hypolimnion was found to be substantial, with a magnitude comparable to ~18% of the hypolimnetic O_2 utilization rate over the whole stratification period (Bouffard et al., 2013).

Horizontal O_2 gradients and associated horizontal advective O_2 fluxes were not quantified in this study. Our data suggest, however, that such fluxes would not significantly contribute to the O_2 balance at the Tommeliten site. BBL O_2 concentration time series (Fig. 5a) did not show any variability at the tidal and or inertial frequencies, implying that horizontal O_2 gradients were small. Additionally, mean currents in the BBL were small (~2 cm s^{-1}) compared to the tidal amplitudes. This, in conjunction with weak horizontal O_2 gradients, suggests that horizontal advective O_2 fluxes during our observational period are negligible compared to the turbulent O_2 flux from the thermocline.

Based on the above, we can argue that the O_2 dynamics during the stratified period are more complicated than previously regarded. To maintain an excess of O_2 in the thermocline, primary producers require adequate nutrient entrainment from the bottom water to fuel potential new production. The resulting increase in (new) productivity and subsequent export to the bottom water could boost the carbon turnover estimates substantially. Using a 1:1 O_2 utilization – carbon re-mineralization (see Canfield, 1993), Greenwood et al. (2010) inferred the average BBL carbon re-mineralization rate at the nearby North Dogger to be 15 mmol m^{-2} d^{-1}, or 180 mg C m^{-2} d^{-1}. Similar results for a typical NW European shelf sea were obtained via modeling by Sharples (2008), who reported rates ranging from ~35 to ~200 mg m^{-2} d^{-1} for neap and spring tide, respectively. Their study, however, did not include the daily tidal variation, and thus rates could be much higher on shorter timescales.

With the absence of targeted long-term studies focusing on O_2 and carbon dynamics in the thermocline and BBL, we can only speculate on the long-term fate of the BBL O_2 and its replenishment from the thermocline by vertical O_2 fluxes (F_θ). It

seems possible that the overall net BBL water column O_2 respiration, R, is higher than previously thought, suggesting a much higher carbon turnover than inferred from the apparent O_2 loss rate. Based on Eq. (6), the BBL carbon re-mineralization (and export to the BBL) would be on the order of nearly 850 mg C m^{-2} d^{-1}, nearly a factor of 5 higher than reported by Greenwood et al. (2010). However, the same turbulent transport that supports the O_2 export from the DCM to the BBL also supports BBL nutrient import to the DCM (Fig. 6). The higher import of nutrients to the DCM likely promotes additional primary production and a subsequent increase in organic matter (OM) export to the BBL. In such a scenario, the transient O_2 flux to the BBL presented in this study will be associated with additional OM to the BBL, and therefore lead to a temporary increased re-mineralization that offsets the increased F_θ. While the overall effect is an increase in carbon turnover, this process would not result in any observable change in the decreasing O_2 trend (apparent O_2 loss rate).

4.3 Causes and controls on BBL O_2 depletion

According to Boers (2005), for BBL O_2 to decrease throughout the stratified season, there must be suitable physical conditions, biomass production, nutrient input and continued benthic O_2 uptake. *SUR*, and thus the sediment nutrient release and organic carbon mineralization have been shown to be strongly tidal-driven (McGinnis et al., 2014). Therefore, we briefly discuss the potential tidal impact driving the overall carbon cycling and suggest factors that may promote the development of lower BBL O_2 concentrations during the stratification period.

Tidal forcing on diapycnal constituent fluxes and primary production have been explored by e.g., Sharples et al. (2007, 2008). The authors showed that spring-neap tide drives nutrient fluxes between the BBL and the DCM at the thermocline, and the carbon export. Based on our velocity measurements and estimated O_2 fluxes, we can expect similar patterns corresponding to semidiurnal tidal fluctuations. Blauw et al. (2012) investigated fluctuating phytoplankton concentrations in relation to tidal drivers and found that in the southern North Sea, chlorophyll fluctuations correlated with the typical tidal current speed periods, the semidiurnal tidal cycle, in addition to the day-night and spring-neap periods. During most of the year, chlorophyll and suspended particulate matter fluctuated in phase with tidal current speed and indicated alternating periods of sinking and vertical mixing of algae and suspended matter with

480 tidal cycles. Thus, these results suggest that in addition to the spring-neap tidal cycles,
481 we can expect a semidiurnal tidal-driven export of carbon and O_2 from the DCM to
482 the BBL, and entrainment of nutrients that strongly vary based on a timescale related
483 to the semi-diurnal tidal cycle.

484 The flux of O_2 from the DCM production zone downward to the BBL could
485 set the lower limit of the BBL O_2 concentration, and thus the O_2 depletion level,
486 during the stratification period. If there is little isolation between the zone of
487 production and the zone of mineralization, then the net O_2 production and O_2
488 utilization would nearly balance. In such case, the apparent O_2 loss in the BBL would
489 either be negligible or very small, depending whether the *SUR*, which is largely
490 particulate organic matter driven, will be balanced by the ventilation from the
491 thermocline. However, historically decreasing BBL O_2 concentrations within the
492 North Sea (Queste et al., 2013) point to an increasing disconnect between the primary
493 O_2 production zone and the mineralization zone. Greenwood et al. (2010) state that
494 stratification is an important factor which determines susceptibility to O_2 depletion,
495 especially in their nearby study site Oyster Grounds.

496 Surveys on the North Sea have shown that the regions with the lowest BBL O_2
497 concentrations are generally characterized by the strongest stratification (see Queste
498 et al., 2013), with the lowest values (~100 μmol kg^{-1}) reported to occur during
499 particularly calm and warm weather (see Boers, 2005; Weston et al., 2008). Strong
500 gradients in the thermocline associated with warmer temperature are suggested to
501 limit the O_2 flux to the BBL (Weston et al., 2008). This points to potential future O_2
502 depletion resulting from increasing temperatures leading to both stronger stratification
503 and a longer stratification season (Lowe et al., 2009). However, it could be argued
504 that if O_2 fluxes between the DCM and BBL were suppressed, then the upward
505 nutrient fluxes would be similarly suppressed, thus inhibiting primary production and
506 reducing the potential for O_2 deficits.
507

508 ## 4.4 Biological perspective

509 The occurrence of stronger stratification and susequently reduced turbulent
510 mixing could alter algal populations (Hickman et al., 2009), potentially favoring
511 migrating/swimming phytoplankton. An example of these migrating phytoplankton
512 species, armored dinoflagellates, are extensively found in the DCM of the central and

513 northern North Sea during the summer months; their abundance was found to be
514 largely determined by the local hydrodynamic conditions (Reid et al., 1990). In calm
515 conditions, which are typically associated with stronger stratification, there are often
516 blooms of migrating dinoflagellates which have access to the large nutrient pool in the
517 deeper water and can out-compete non-migrating species for both light and nutrients.
518 Stronger turbulent mixing, in contrast, has been suggested to interfere with their
519 swimming abilities (see Jephson et al., 2012 and references therein).

520 Algal migration could promote an upward shift of the DCM and move the
521 associated O_2 production higher in the thermocline where turbulence levels are
522 reduced, while still maintaining comparable production rates. Even by a few meters,
523 such an upward shift would substantially reduce turbulent O_2 fluxes to the BBL and
524 likely further isolate the BBL from the potential O_2 supply in the thermocline,
525 although maintaining similar rates of carbon export (settling armored dinoflagellates).
526 Studies on climate change impacts on the North Sea have suggested that O_2 loss in the
527 bottom waters would mainly result from a strengthening of the stratification and O_2
528 solubility reduction with increasingly warmer waters (e.g., Meire et al., 2013). In
529 those scenarios, the intricate interplay between local tidally-driven processes, water
530 column structure, biogeochemical cycling and active phytoplankton migration have
531 not been considered nor quantified. The proposed mechanism could contribute to the
532 observed decreasing O_2 levels in the North Sea water column, however, further
533 detailed studies are obviously necessary to validate and fully quantify this effect, and
534 the results described in this study, at the seasonal level.
535

536 **Acknowledgements**

537 We are thankful to the captain and crewmembers of the R/V *Celtic Explorer*
538 for their outstanding collaboration and support during the survey, Uwe Koy and
539 Rudolf Link for their logistic support, and Jens Schafstall, Tim Fischer and Markus
540 Faulhaber for their help in data collection and processing. We are grateful for the
541 technical development and support in deployment of the benthic chamber by Ralf
542 Schwarz, Sergiy Cherednichenko and the ROV Kiel 6000 team. Financial support was
543 provided by the Sonderforschungsbereich (SFB) 754 “Climate – Biogeochemisty in
544 the tropical Ocean”, SFB 574 “Volatiles and Fluids in Subduction Zones”, and by the
545 Excellence Cluster “Future Ocean” (project 2009/1 CP 0915, LR), supported by the

546 Deutsche Forschungsgemeinschaft (DFG). Additional founding was provided by the
547 National Environmental Research Council (NERC, project NE/J011681/1). The cruise
548 was financed by Wintershall within the Fluid and Gas Seepage in the Southern
549 German North Sea (SDNS) project.
550

References

Batchelor, G. K.: The theory of homogeneous turbulence, Cambridge University Press, Cambridge, 1953.

Best, M. A., Wither, A. W., and Coates, S.: Dissolved oxygen as a physico-chemical supporting element in the Water Framework Directive, Mar. Pollut. Bull., 55, 53–64, doi:10.1016/j.marpolbul.2006.08.037, 2005.

Blauw, A. N., Beninca, E., Laane, R. W. P. M., Greenwood, N., and Huisman, J.: Dancing with the tides: fluctuations of coastal phytoplankton orchestrated by different oscillatory modes of the tidal cycle, Plos One, 7, e49319, doi:10.1371/journal.pone.0049319, 2012.

Boers, M.: Effects of a deep sand extraction pit. Final report of the PUTMOR measurements at the Lowered Dump Site, Rijkswa- terstaat, The Netherlands, RIKZ/2005.001, 87, 2005.

Bouffard, D., Ackerman, J. D., and Boegman, L.: Factors affecting the development and dynamics of hypoxia in a large shallow stratified lake: hourly to seasonal patterns, Water Resour. Res., 49, 2380–2394, doi:10.1002/wrcr.20241, 2013.

Brandt, P., Bange, H., Banyte, D., Dengler, M., Didwischus, S-H., Fischer, T., Greatbatch, R., Hahn, J., Kanzow, T., Karstensen, J., Körtzinger, A., Krahmann, G., Schmidtko, S., Stramma, L., Tanhua T., and Visbeck, M.: On the role of circulation and mixing in the ventilation of oxygen minimum zones with a focus on the eastern tropical North Atlantic, Biogeosciences, 12, 489–512, doi:10.5194/bg-12-489-2015, 2015.

Burchard, H., and Rippeth, T. P.: Generation of bulk shear spikes in shallow stratified tidal seas, J. Phys. Oceanogr., 39, 969–985, doi:10.1175/2008JPO4074.1, 2009.

Canfield, D. E.: Organic matter oxidation in marine sediments, in: Interactions of C, N, P and S biogeochemical cycles and global change, edited by: Wollast, R., Mackenzie, F. T., and Chou, L., Springer, Berlin, 333–363, 1993.

Chan, F., Barth, J. A., Lubchenco, J., Kirincich, A., Weeks, H., Peterson, W. T., and Menge, B. A.: Emergence of anoxia in the California current large marine ecosystem, Science, 319, 920–920, doi:10.1126/Science.1149016, 2008.

581 Crawford, W. R., and Pena, M. A.: Declining oxygen on the British Columbia
582 continental shelf, Atmos. Ocean., 51, 88–103, doi:10.1080/07055900.2012.753028,
583 2013.

584 Diaz, R. J.: Overview of hypoxia around the world, J. Environ. Qual., 30, 275–281,
585 doi:10.2134/jeq2001.302275x, 2001.

586 Diaz, R. J., and Rosenberg, R. : Spreading dead zones and consequences for marine
587 ecosystems, Science, 321, 926–929, doi:10.1126/Science.1156401, 2008.

588 Dohan, K, and Davis, R. E.: Mixing in the transition layer during two storm events, J.
589 Phys. Oceanogr., 41, 42–66, doi:10.1175/2010jpo4253.1, 2011.

590 Efron, B.: 1977 Rietz lecture - bootstrap methods - another look at the jackknife, Ann.
591 Stat., 7, 1–26, 1979.

592 Ferrari, R., and Boccaletti, G.: Eddy-mixed layer interactions in the ocean,
593 Oceanography, 17, 12–21, doi:10.5670/oceanog.2004.26. 2004.

594 Ferrari, R., and Polzin, K. L.: Finescale structure of the T-S relation in the eastern
595 North Atlantic, J. Phys. Oceanogr., 35, 1437–1454, doi:10.1175/JPO2763.1, 2005.

596 Fischer, T., Banyte, D., Brandt, P., Dengler, M., Krahmann, G., Tanhua, T., and
597 Visbeck, M.: Diapycnal oxygen supply to the tropical North Atlantic oxygen
598 minimum zone, Biogeosciences, 10, 5079–5093, doi:10.5194/bg-10-5079-2013, 2013.

599 Fofonoff, N. P.: Physical properties of seawater: A new salinity scale and equation of
600 state for seawater, J. Geophys. Res., 90, 3332–3342, doi:10.1029/Jc090ic02p03332,
601 1985.

602 Glud, R. N.: Oxygen dynamics of marine sediments, Mar. Biol. Res., 4, 243–289,
603 doi:10.1080/17451000801888726, 2008.

604 Grantham, B. A., Chan, F., Nielsen, K. J., Fox, D. S., Barth, J. A., Huyer, A.,
605 Lubchenco, J., and Menge, B. A.: Upwelling-driven nearshore hypoxia signals
606 ecosystem and oceanographic changes in the northeast Pacific, Nature, 429, 749–754,
607 doi:10.1038/Nature02605, 2004.

608 Greenwood, N., Parker, E. R., Fernand, L., Sivyer, D. B., Weston, K., Painting, S. J.,
609 Kroger, S., Forster, R. M., Lees, H. E., Mills, D. K., and Laane, R. W. P. M.:
610 Detection of low bottom water oxygen concentrations in the North Sea; implications

611 for monitoring and assessment of ecosystem health, Biogeosciences, 7, 1357–1373,
612 doi:10.5194/bg-7-1357-2010, 2010.

613 Hickman, A. E., Holligan, P. M., Moore, C. M., Sharples, J., Krivtsov, V., and
614 Palmer, M. R.: Distribution and chromatic adaptation of phytoplankton within a shelf
615 sea thermocline, Limnol. Oceanogr., 54, 525–536, doi:10.4319/lo.2009.54.2.0525,
616 2009.

617 Hovland, M., and Judd, A.: Seabed pockmarks and seepage: Impact on geology,
618 biology and the marine environment, Graham and Trotman, London, 1988.

619 Itsweire, E. C., Osborn, T. R., and Stanton, T. P.: Horizontal distribution and
620 characteristics of shear layers in the seasonal thermocline, J. Phys. Oceanogr., 19,
621 302–320, doi:10.1175/1520-0485(1989)019<0301:HDACOS>2.0.CO;2, 1989.

622 Ivey, G. N., and Imberger, J.: On the nature of turbulence in a stratified fluid, Part I:
623 The energetics of mixing, J. Phys. Oceanogr., 21, 650–658, doi:10.1175/1520-
624 0485(1991) 021<0650:OTNOTI>2.0.CO;2, 1991.

625 Jephson, T., Carlsson, P., and Fagerberg, T.: Dominant impact of water exchange and
626 disruption of stratification on dinoflagellate vertical distribution, Estuarine, Coastal
627 Shelf Sci., 112, 198–206, doi:10.1016/j.ecss.2012.07.020, 2012.

628 Jørgensen, B. B., and Revsbech, N. P.: Diffusive boundary layers and the oxygen
629 uptake of sediments and detritus, Limnol. Oceanogr., 30, 111–122,
630 doi:10.4319/lo.1985.30.1.0111, 1985.

631 Kemp, W. M., Testa, J. M., Conley, D. J., Gilbert, D., and Hagy, J. D.: Temporal
632 responses of coastal hypoxia to nutrient loading and physical controls,
633 Biogeosciences, 6, 2985–3008, doi:10.5194/bg-6-2985-2009, 2009.

634 Knight, P. J., Howarth, M. J., and Rippeth, T. P.: Inertial currents in the northern
635 North Sea, J. Sea Research, 47, 269–284, doi:10.1016/S1385-1101(02)00122-3, 2002.

636 Kreling, J., Bravidor, J., McGinnis, D. F., Koschorreck, M., and Lorke, A.: Physical
637 controls of oxygen fluxes at pelagic and benthic oxyclines in a lake, Limnol.
638 Oceanogr., 59, 1637–1650, doi:10.4319/lo.2014.59.5.1637, 2014.

639 Lorke, A., Umlauf, L., and Mohrholz, V.: Stratification and mixing on sloping
640 boundaries, Geophys. Res. Lett., 35, L14610, doi:10.1029/2008GL034607, 2008.

641 Lowe, J. A., Howard, T. P., Pardaens, A., Tinker, J., Holt, J., Wakelin, S., Milne, G.,
642 Leake, J., Wolf, J., Horsburgh, K., Reeder, T., Jenkins, G., Ridley, J., Dye, S., and
643 Bradley, S.: UK Climate Projections science report: Marine and coastal projections.
644 Met Office Hadley Centre, available at:
645 http://ukclimateprojections.metoffice.gov.uk/22530, 2009.

646 MacKinnon, J. A., and Gregg, M. C.: Near-inertial waves on the New England shelf:
647 The role of evolving stratification, turbulent dissipation, and bottom drag, J. Phys.
648 Oceanogr., 35, 2408–2424, doi:10.1175/JPO2822.1, 2005.

649 McGinnis, D. F., Sommer, S., Lorke, A., Glud, R. N., and Linke, P.: Quantifying
650 tidally driven benthic oxygen exchange across permeable sediments: An aquatic eddy
651 correlation study, J. Geophys. Res.: Oceans, 119, 6918–6932,
652 doi:10.1002/2014JC010303, 2014.

653 Meire, L., Soetaert, K. E. R., and Meysman, F. J. R.: Impact of global change on
654 coastal oxygen dynamics and risk of hypoxia, Biogeosciences, 10, 2633–2653,
655 doi:10.5194/bg-10-2633-2013, 2013.

656 Meyer, E. M. I., Pohlmann, T., and Wiesse, R.: Thermodynamic variability and
657 change in the North Sea (1948-2007) derived from a multidecadal hindcast, J. Mar.
658 Syst., 86, 35–44, doi:10.1016/j.jmarsys.2011.02.001, 2011.

659 Neubacher, E. C., Parker, R. E., and Trimmer, M.: Short-term hypoxia alters the
660 balance of the nitrogen cycle in coastal sediments, Limnol. Oceanogr., 56, 651–665,
661 doi:10.4319/lo.2011.56.2.0651, 2011.

662 North Sea Task Force: North Sea Quality Status Report, Report No.: 1 872349 05 6,
663 London: Oslo and Paris Commissions, 1993.

664 Osborn, T. R.; Estimates of the local rate of vertical diffusion from dissipation
665 measurements, J. Phys. Oceanogr., 10, 83–89, doi:10.1175/1520-
666 0485(1980)010<0083: EOTLRO>2.0.CO;2, 1980.

667 OSPAR (Oslo-Paris convention for the protection of the marine environment of the
668 North-East Atlantic): EcoQO Handbook—Handbook for the application of ecological
669 quality objectives in the North Sea, Report No.: 978-1-905859-46-7, 2nd edn.,
670 OSPAR Biodiversity Series 2009/307, available at
671 http://www.ospar.org/v_publications/browse.asp, 2009.

672 OSPAR: Quality Status Report 2010, Report No: 978-1-906840-44-0, OSPAR
673 Commission, London, available at http://qsr2010.ospar.org/en/index.html, 2010.

674 Otto, L., Zimmerman, J. T. F., Furnes, G. K., Mork, M., Saetre, R., and Becker, G.:
675 Review of the physical oceanography of the North Sea, Ned. J. Sea Res., 26, 161–
676 238, doi:10.1016/0077-7579(90)90090-4, 1990.

677 Palmer, M. R., Rippeth, T. P., and Simpson, J. H.: An investigation of internal mixing
678 in a seasonally stratified shelf sea, J. Geophys. Res., 113, C12005,
679 doi:10.1029/2007JC004531, 2008.

680 Pfannkuche, O., Linke, P.: GEOMAR landers as long-term deep-sea observatories,
681 Sea Technol. 44, 50–55, 2003.

682 Pingree, R. D., Holligan, P. M., and Mardell, G. T.: The effect of vertical stability on
683 phytoplankton distributions in the summer on the Northwest European Shelf, Deep
684 Sea Res., 25, 1011–1028, doi:10.1016/0146-6291(78)90584-2, 1978.

685 Prandke, H., and Stips, A.: Test measurements with an operational microstructure-
686 turbulence profiler: Detection limit of dissipation rates, Aquat. Sci., 60, 191–209,
687 doi:10.1007/s000270050036, 1998.

688 Queste, B.Y., Fernand, L., Jickells, T. D., and Heywood, K. J.: Spatial extent and
689 historical context of North Sea oxygen depletion in August 2010, Biogeochemistry,
690 113, 53–68, doi:10.1007%2Fs10533-012-9729-9, 2013.

691 Radach, G. and Lenhart, H. J.: Nutrient dynamics in the North Sea: Fluxes and
692 budgets in the water column derived from ERSEM, Neth. J. Sea Res., 33, 301–335,
693 doi:10.1016/0077-7579(95)90051-9, 1995

694 Reid, P. C., Lancelot, C., Gieskes, W. W. C., Hagmeier, E., and Weichart, G.:
695 Phytoplankton of the North Sea and its dynamics - a review, Neth. J. Sea Res., 26,
696 295–331, doi:10.1016/0077-7579(90)90094-W, 1990.

697 Rhein, M., Dengler, M., Sültenfuß, J., Hummels, R., Hüttl-Kabus, S., and Bourles, B.:
698 Upwelling and associated heat flux in the equatorial Atlantic inferred from helium
699 isotope disequilibrium, J. Geophys. Res., 115, C08021, doi:10.1029/2009JC005772,
700 2010.

701 Rippeth, T. P.: Mixing in seasonally stratified shelf seas: A shifting paradigm, Phil.
702 Trans. R. Soc. A, 363, 2837–2854, doi:10.1098/rsta.2005.1662, 2005.

703 Rippeth, T. P., Simpson, J. H., Player, R., and Garcia, M. C.: Current oscillations in
704 the diurnal-inertial band on the Catalonian Shelf in spring, Cont. Shelf Res., 22, 247–
705 265, doi:10.1016/S0278-4343(01)00056-5, 2002.

706 Rippeth, T. P., Wiles, P., Palmer, M. R., Sharples, J., and Tweddle, J.: The diapcynal
707 nutrient flux and shear-induced diapcynal mixing in the seasonally stratified western
708 Irish Sea, Cont. Shelf Res., 29, 1580–1587, doi:10.1016/j.csr.2009.04.009, 2009.

709 Schafstall, J., Dengler, M., Brandt, P., and Bange, H.: Tidal-induced mixing and
710 diapycnal nutrient fluxes in the Mauritanian upwelling region, J. Geophys. Res.:
711 Oceans, 115, C10014, doi:10.1029/2009jc005940, 2010.

712 Sharples, J.: Potential impacts of the spring-neap tidal cycle on shelf sea primary
713 production, J. Plankton Res., 30, 183–197, doi: 10.1093/plankt/fbm088, 2008.

714 Sharples, J., Moore, C. M., Rippeth, T. P., Holligan, P. M., Hydes, D. J., Fisher, N.
715 R., and Simpson, J. H.: Phytoplankton distribution and survival in the thermocline,
716 Limnol. Oceanogr., 46, 486–496, doi:10.4319/lo.2001.46.3.0486, 2001.

717 Sharples, J., Tweddle, J. F., Green, J. A. M., Palmer, M. R., Kim, Y. N., Hickman, A.
718 E. Holligan, P. M., Moore, C. M., Rippeth, T. P., Simpson, J. H., and Krivtsov, V.:
719 Spring-neap modulation of internal tide mixing and vertical nitrate fluxes at a shelf
720 edge in summer, Limnol. Oceanogr., 52, 1735–1747, doi: 10.4319/lo.2007.52.5.1735,
721 2007.

722 Schneider von Deimling, J., Greinert, J., Chapman, N. R., Rabbel, W., and Linke, P.:
723 Acoustic imaging of natural gas bubble ebullition in the North Sea: Sensing the
724 temporal, spatial and activity variability, Limnol. Oceanogr.: Methods, 8, 155–171,
725 doi:10.4319/ lom.2010.8.155, 2010.

726 Shih, L. H., Koseff, J. R., Ivey, G. N., and Ferziger, J. H.: Parameterization of
727 turbulent fluxes and scales using homogeneous sheared stably stratified turbulence
728 simulations, J. Fluid Mech., 525, 193–214, doi:10.1017/S0022112004002587, 2005.

729 Simpson, J. H., and Tinker, J. P.: A test of the influence of tidal stream polarity on the
730 structure of turbulent dissipation, Cont. Shelf Res., 29, 320–332, doi:10.1016/
731 j.csr.2007.05.013, 2009.

732 Smyth, W. D., Moum, J. N., and Caldwell, D. R.: The efficiency of mixing in
733 turbulent patches: inferences from direct simulations and microstructure observations,

734 J. Phys. Oceanogr., 31, 1969–1992, doi:10.1175/1520-
735 0485(2001)031<1969:TEOMIT>2.0.CO;2, 2001.

736 St. Laurent, L., and Schmitt, R. W.: The contribution of salt fingers to vertical mixing
737 in the North Atlantic Tracer Release Experiment, J. Phys. Oceanogr., 29, 1404–1424,
738 1999.

739 Thomas, H., Bozec, Y., de Baar, H. J. W., Elkalay, K., Frankignoulle, M.,
740 Schiettecatte, L.-S., Kattner, G., and Borges, A. V.: The carbon budget of the North
741 Sea, Biogeosciences, 2, 87–96, doi:10.5194/bg-2-87-2005, 2005.

742 van Haren, H., Mass, L., Zimmerman, J. T. R., Ridderinkhof, H., and Malschaert, H.:
743 Strong inertial currents and marginal internal wave stability in the central North Sea,
744 Geophys. Res. Lett., 26, 2993–2996, doi:10.1029/1999GL002352, 1999.

745 Vaquer-Sunyer, R., and Duarte, C. M.: Thresholds of hypoxia for marine biodiversity,
746 P. Natl. Acad. Sci. USA., 105, 15452–15457, doi:10.1073/pnas.0803833105, 2008.

747 Wanninkhof, R.: Relationship between wind speed and gas exchange over the ocean,
748 J. Geophys. Res.: Oceans, 97, 7373–7382, doi:10.1029/92jc00188, 1992

749 Weston, K., Fernand, L., Mills, D. K., Delahunty, R., and Brown, J.: Primary
750 production in the deep chlorophyll maximum of the central North Sea, J. Plankton
751 Res., 27, 909–922, doi:10.1093/plankt/fbi064, 2005.

752 Weston, K., Greenwood, N., Fernand, L., Pearce, D. J., and Sivyer, D. B.:
753 Environmental controls on phytoplankton community composition in the Thames
754 plume, U.K. J. Sea Res., 60, 246–254, doi:10.1016/j.seares.2008.09.003, 2008.

755 Winkler, L., Die Bestimmung des in Wasser Gelösten Sauerstoffes, Berichte der
756 Deutschen Chemischen Gesellschaft, **21,** 2843–2855, 1888.
757

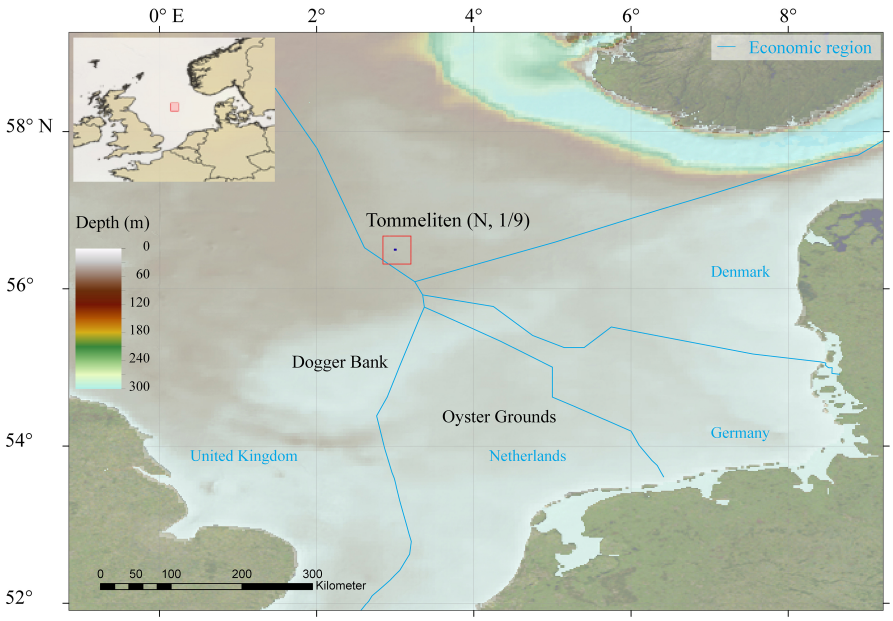

Figure 1. Map of the North Sea indicating the water depths and location of the Tommeliten site and the borders of the economic regions of the surrounding European countries.

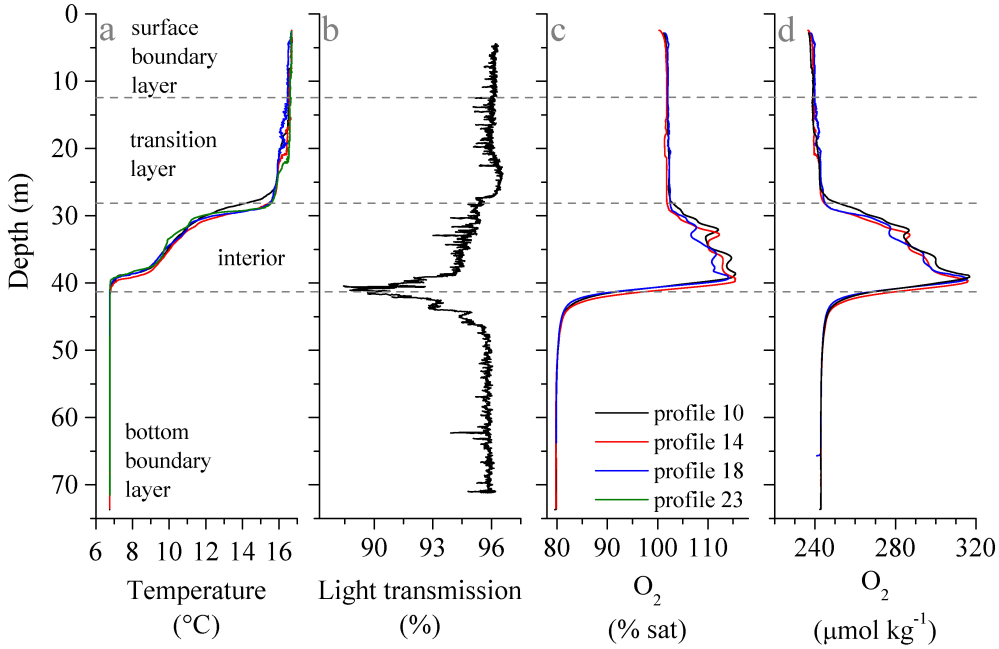

Figure 2. Selected water column profiles based on based on high-resolution MSS profiles (a, c, d) and ship CTD profile (b). (a) Potential temperature profiles. Water column layers were identified based on the temperature profiles. A 0.2°C and 1.5°C decrease from the surface boundary layer average temperature (3–6 m depth) was used determine the depth of the surface boundary layer – transition layer interface and the transition layer – interior interface, respectively. Correspondingly, a 0.2°C from a 50-60 m depth average temperature was used to locate the interior – bottom boundary layer interface. (b) Light transmission profile. (c, d) O_2 saturation profiles and associated absolute concentrations.

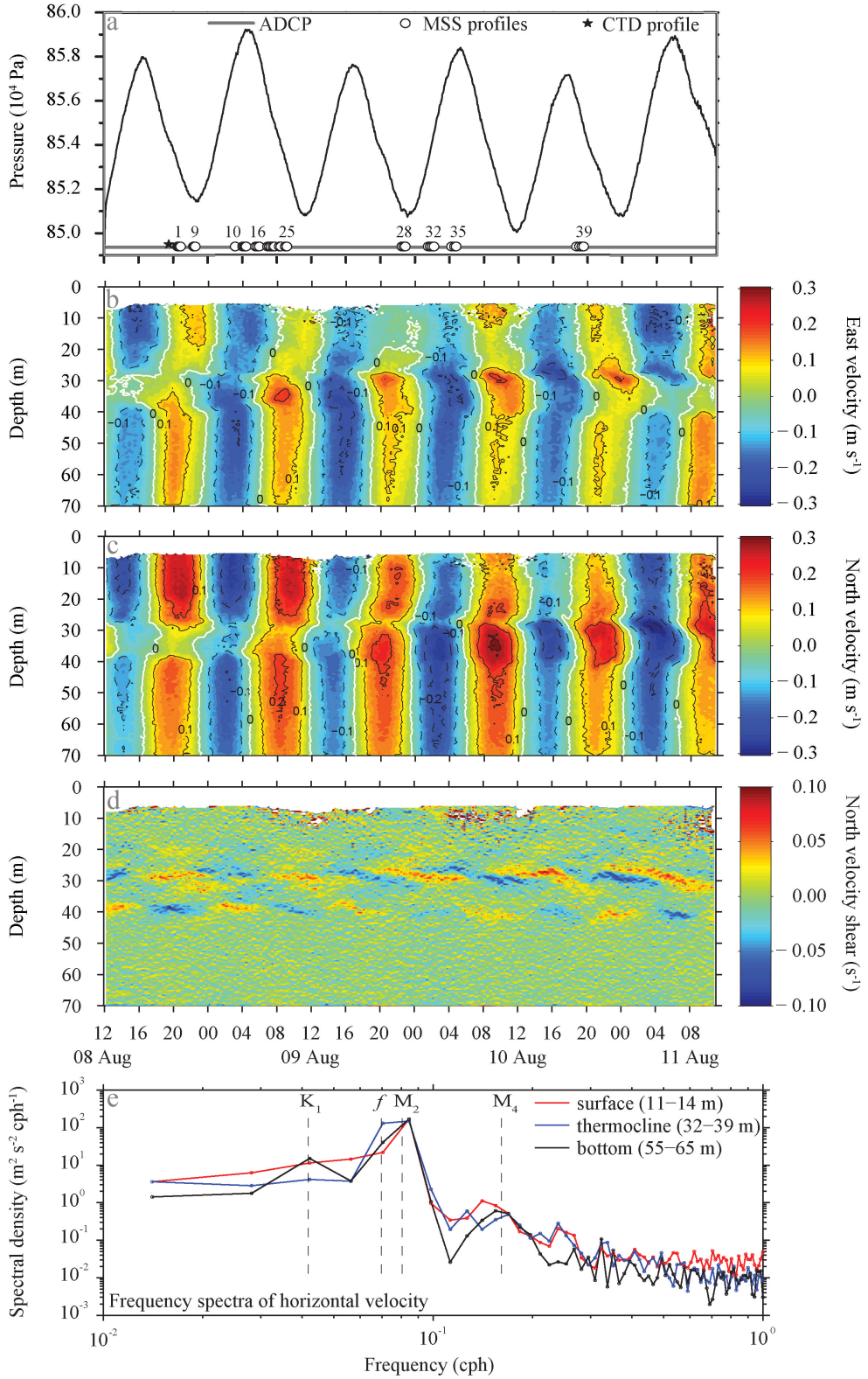

774

775

776 Figure 3. Current regime at the Tommeliten site from ADCP measurements (a - d)
777 and spectral analysis (e). (a) Sea surface elevation relative to average level during the
778 observational period (elevation = 0 m) and schedule of different instrument

779 deployments. Numbers on the MSS markers indicate the profile number. (b, c)
780 Horizontal velocities, showing 20 min averaged east (b) and north (c) velocities. (d)
781 Vertical shear of North velocity, *dv/dz*, calculated from the ADCP velocity data (see
782 panels b, c). Note that panels a - d have the same time axis. (e) Frequency spectra of
783 horizontal velocity calculated from the ADCP data for selected depth ranges for the
784 SBL (surface; red line), thermocline (blue line), and BBL (bottom; black line). The
785 inertial *f,* K_1, M_2 and M_4 frequencies are marked.

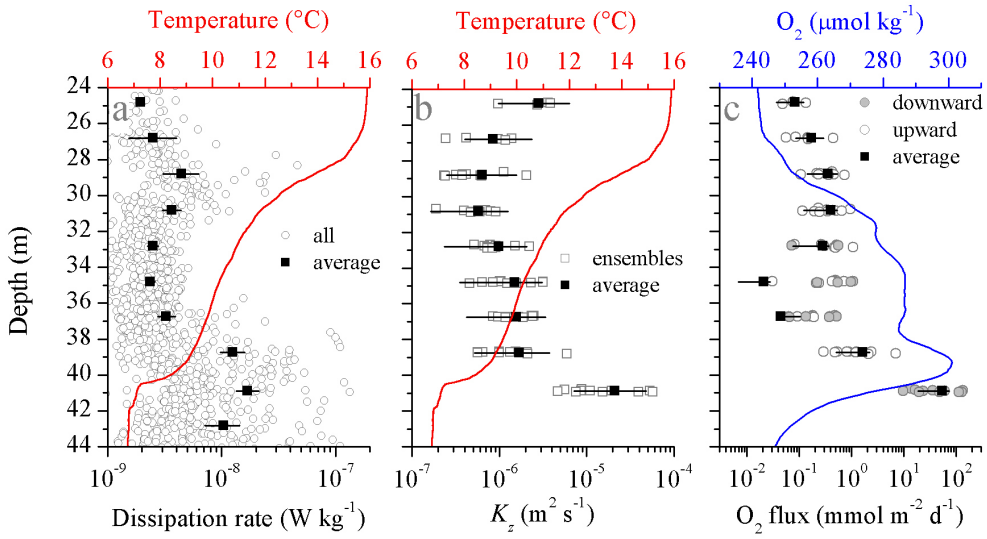

786
787

788 Figure 4. Overview of turbulent transport and O_2 fluxes within the interior (defined in
789 Fig. 2). Each panel is overlaid with temperature (a, b) and O_2 concentration (c)
790 profiles. (a) Dissipation from all profiles (open dots) together with the arithmetic
791 mean (solid squares). (b) Average vertical eddy diffusion coefficient K_z with
792 uncertainties bars and the K_z values for every ensemble (open squares), which
793 represent the average over 3 to 4 consecutive profiles. (c) Calculated average O_2 flux
794 over 2 m bins with the respective uncertainties intervals (solid square and black line).
795 The values for each profile cluster are shown both downward and upward fluxes (grey
796 solid and open dots, respectively). Note that in the center interior (33 – 37 m) the
797 average reflects the combination of the variability of the observed upward and
798 downwards fluxes.
799

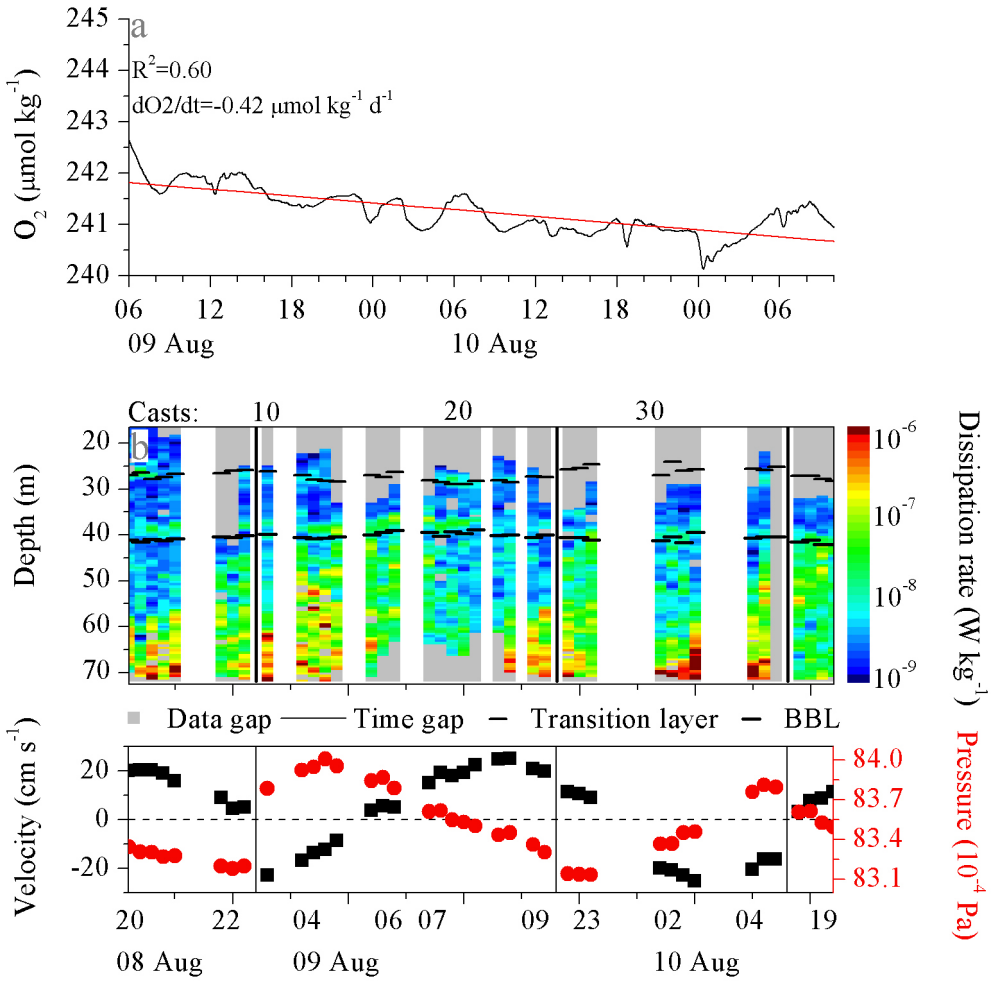

Figure 5. BBL dissolved oxygen time series and turbulence contour. (a) Near-seafloor BBL O_2 concentration changes over the observational period from the POZ-Lander. Red line indicates the estimated apparent linear O_2 loss. (b, top) Turbulence contour plot of all MSS90 casts together with the temperature layers. Thin and thick dashed lines represent the transition layer – interior interface and the interior – BBL interface, respectively. Gray spots indicate data missing due to uncompleted profiles (casts 16-23), unsuccessful profiles (cast 36), or flagged as bad based on spikes, collisions and suspected contamination due to ship activity. The vertical black lines indicate the transition (time gaps) between consecutive profile ensembles. (b, bottom) Background information on bottom current, and hydrostatic pressure during the casts. Both velocity and pressure data were collected by the deployed POZ lander. Note that as a result of the time gaps between the consecutive MSS90 casts (see Fig. 3a) the time scale is not linear.

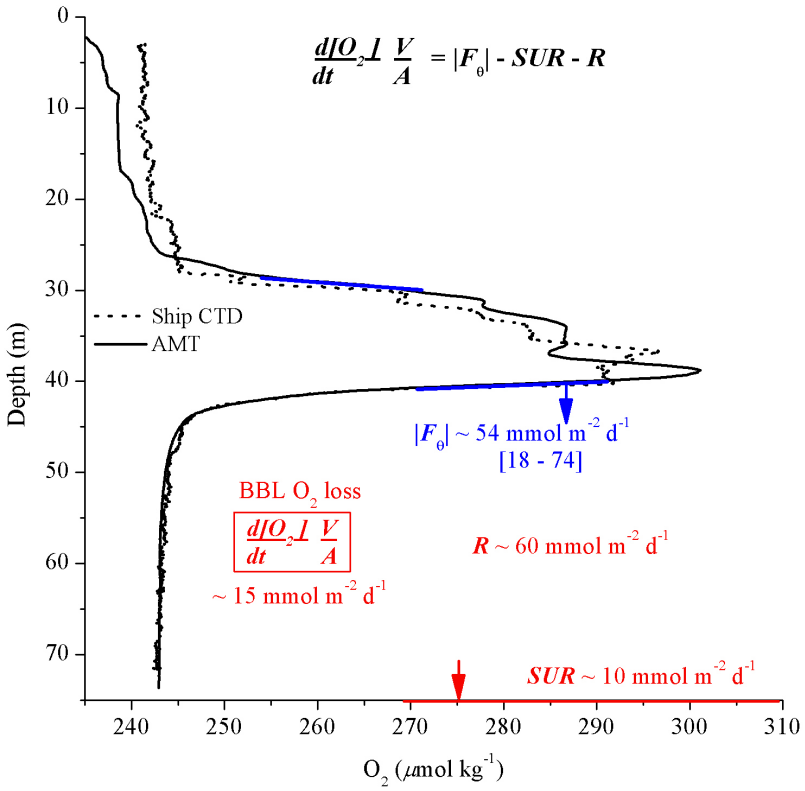

Figure 6. Main O_2 fluxes in this study. The ranges shown for the interior O_2 fluxes refer to the associated uncertainty and intermittency levels. The sediment O_2 uptake rates (SUR) are based on eddy correlation (EC) measurements (McGinnis et al., 2014), while central North Sea apparent BBL O_2 loss is based on Greenwood et al. (2010) and this study. Representative O_2 profiles are based on the AMT sensor on the MSS profiler (solid line) and ship CTD (dotted line). Note that while the O_2 profiles showed differences in absolute concentration within the thermocline, the actual O_2 gradients within the thermocline-BBL oxycline are comparable.